

4.2 K Sensitivity-Tunable Radio Frequency Reflectometry of a Physically Defined p-channel Silicon Quantum Dot

Sinan Bugu,^{1, a)} Shimpei Nishiyama,¹ Kimihiko Kato,² Yongxun Liu,² Shigenori Murakami,² Takahiro Mori,² Thierry Ferrus,³ and Tetsuo Kodera^{1, b)}

¹⁾ Tokyo Institute of Technology 2-12-1 Ookayama, Meguro-ku, Tokyo 152-8552, Japan

²⁾ Device Technology Research Institute (D-Tech), National Institute of Advanced Industrial Science and Technology (AIST), Central 2, 1-1-1 Umezono, Tsukuba, Ibaraki, 305-8568, Japan

³⁾ Hitachi Cambridge Laboratory, J. J. Thomson Avenue, CB3 0HE, Cambridge, United Kingdom

(Dated: 5 June 2022)

We demonstrate the measurement of p-channel silicon-on-insulator quantum dots at liquid helium temperatures by using a radio frequency (rf) reflectometry circuit comprising of two independently tunable GaAs varactors. This arrangement allows observing Coulomb diamonds at 4.2 K under nearly best matching condition and optimal signal-to-noise ratio. We also discuss the rf leakage induced by the presence of the large top gate in MOS nanostructures and its consequence on the efficiency of rf-reflectometry. These results open the way to fast and sensitive readout in multi-gate architectures, including multi qubit platforms.

Hole spins confined in silicon structures have attracted considerable attention due to their ability to provide quantum bit architectures with a longer coherence¹ and faster gate operation times² compared to electrons in III-V materials³. They also take advantage of an all electric field control due to the increase in the spin-orbit coupling strength⁴⁻⁷, a charge offset stability⁸ necessary for scalability purposes as well as a necessary compatibility with current industry production lines in view of commercialisation.⁹⁻¹¹. However, to take full advantage of these properties in the view of quantum computing applications, one requires to deal with the combination of a large impedance either at the device or at the measurement unit with a large capacitance, which provides an effective low-pass filter circuit that reduces the bandwidth significantly.¹²

Reflectometry techniques in the radio frequency (rf) range have been developed to circumvent the inherent limitation in bandwidth by incorporating the device into an LC resonant circuit and measuring the modulated reflected signal at a frequency close to the resonant condition¹³. In quantum dot architectures, such a circuit can be integrated either at the sensor, for example a single electron transistor or quantum point contact close to the device to measure¹⁴⁻¹⁷, or directly at one of the control gate of the device itself¹⁸⁻²⁵. Both techniques have proven to be reliable with bandwidths in excess of 10 MHz and are particularly suited to quantum dots where the low-stray parasitic capacitance, generally lower than 1 pF, allows the use of moderate inductance sizes and values to obtain a high resonance frequency and retain good impedance matching. Gated devices including double gate stacks^{26,27} provide a significant advantage in terms of charge noise screening, uniformity of the 2DEG compared with similar but doped structures. However, such advantages can be overcome by the formation of a low impedance leakage pathway to the ground for the rf signal that results from the large parasitic capacitance between the accumulation gate and the two-dimensional electron gas (2DEG)^{17,28,29}. This is particularly severe for the area larger than a few tens of μm^2 ³⁰.

Aside bandwidth considerations, the reduction in the readout integration time has important implications. It allows improving readout fidelity once reaching timescales typically shorter than the relaxation time of the system T_1 and envisioning surface code-based

^{a)} Electronic mail: bugu.s.aa@m.titech.ac.jp

^{b)} Electronic mail: kodera.t.ac@m.titech.ac.jp

applications when measurements become much faster than the coherence time T_2 . However, shorter integration times unequivocally implies a reduction in the signal-to-noise ratio (SNR)³¹. In the low-signal regime, when the changes in the ratio of resistance to capacitance are small, the SNR depends on the coupling coefficient^{32,33} that becomes maximum at perfect matching condition. In order to achieve a high sensitivity while keeping up to perfect impedance matching, voltage-controlled capacitors, or varactors, are generally incorporated into the resonant circuit. Such an implementation has already been used to tune in-situ the resonant frequency of a quantum point contact at 1.8 K³⁴. Similarly, a couple of varactors have been used for impedance matching purposes to measure both the charge sensitivity and the impedance of a quantum dot at 1 K³². More recently, a high-quality resonator with low parasitic capacitance was combined with varactors to improve significantly the charge sensitivity in the range of 55 mK to 1.5 K³³. Such a limitation in the use of rf reflectometry in certain architectures can be severe in p-channel silicon devices due to their lower mobilities compared with n-type devices. This generates an excess resistance in the 2DHG and decreases the readout sensitivity rendering rf measurements more challenging. In this study, we purposely use p-channel Metal-Oxide-Semiconductor (PMOS) devices to demonstrate such an rf leakage effect induced by the top gate and discuss the ability to perform rf reflectometry.

Scanning electron microscope (SEM) image and schematic image of the device are shown in Fig. 1(a) and 1(b), respectively. All devices were fabricated from an undoped 40-nm-thick silicon-on-insulator (SOI) with a 145-nm-thick buried oxide. Quantum dot structures and sides gates were then formed by etching the silicon active layer at selected regions using inductive coupled plasma reactive ion etching (ICP-RIE)^{30,35-37}. After a standard RCA clean, a 3-nm-thick thermal oxide layer was grown with dry oxidation at 850° before the deposition of a 65-nm-thick gate oxide. A top gate made from highly phosphorus-doped polysilicon at a concentration of 10^{-20} cm^{-3} was then deposited. Two devices are used in our study, both having the same structure but different top gate areas, one with a surface area of $0.09 \mu\text{m}^2$ (device 1) and the other with an area of $1 \mu\text{m}^2$ (device 2).

Experiments are performed using the setup shown in Fig. 2. Figures 2(a) and (b) are the setups for the measurement performed at room temperature while Fig. 2(c) is for 4.2 K measurement. RF signal passing through directional coupler is attenuated with a -40 dB attenuator before sent to the quantum dot with a tank circuit. Charge transition in the quantum dot causes a change in the amplitude of the reflected signal. Then, the reflected signal is amplified with room temperature amplifiers, which have a gain of 60-dB in total. Whether to use the setup (a) or (b) depends on the measurement, the signal is sent to part a or part b of the setup depending on the measurement. For the resonant circuit, we use a GaAs double varactor (a Macom MA46H202-1056 for C_m and a Macom MA46H204-1056 for C_t) to tune both the resonance frequency to the region of operation and the impedance matching. This allows us to read out the charge states of a PMOS quantum dot at 4.2 K, under high SNR and tuned matching conditions. When we measure device 1 we add a matching capacitor C_m and a decoupling capacitor C_d ($\sim 24 \text{ pF}$) at the input point of the matching circuit. The purpose of C_d is to increase the quality factor Q of the circuit by decoupling it from the input. The varactor C_t controlled by V_t , aims at controlling the resonant frequency f_r and the loaded impedance Z_L . The second varactor C_m , controlled by V_m mostly controls the value of Z_L and hence the sensitivity (see S2). The rf signal was added via a bias tee to the drain of the device with all the electronic components mounted on a standard FR4 printed circuit board (see S1).

In the rf experiments, the choice for the probing frequency f_c is typically dictated by both noise and circuit impedance considerations. To maintain a high SNR, f_c should always exceed the $1/f$ noise caused by charge fluctuations¹³. On the other hand, if the rf signal is connected to the leads and to avoid leakage of the rf signal, the impedance of the matching circuit Z_m shall not be much larger than the gate impedance $Z_g = 1/2\pi i f_c C_g$ where C_g is the parasitic capacitance of the gate. Such a leakage effect is well demonstrated in the device with the larger gate area (device 2) by exploring its rf response at different carrier frequencies and so, at different values of the resonant circuit inductance. We first determined the parasitic capacitance C_p of the tank circuit by monitoring the variation of the resonance

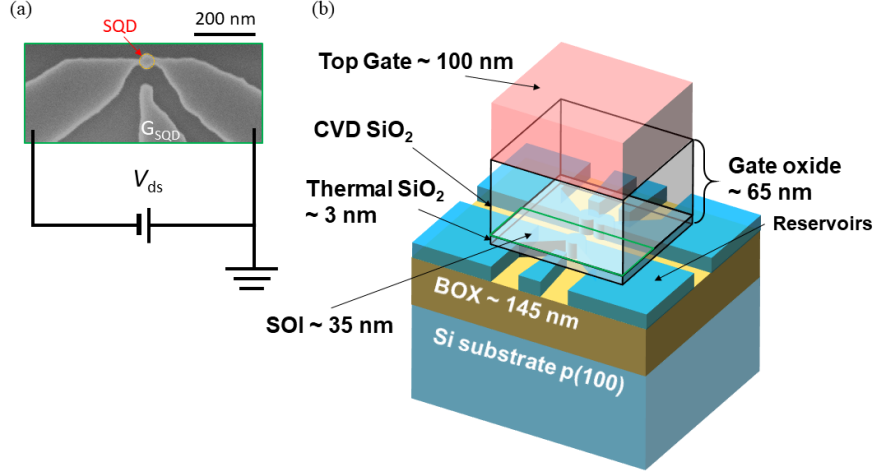


FIG. 1. Device structure. (a) Scanning electron microscope (SEM) image of the device after reactive ion etching. Darkest areas are parts of the SOI that have been etched away whereas the island at the centre is the quantum dot under study with its associated control gate G_{SQD} , (b) Device internal structure once fully processed.

frequency $f_r = 1/2\pi\sqrt{LC_p}$ with changing the inductance value L . We obtain $C_p \sim 0.48$ pF. Several inductors were then used to obtain a set of resonant frequencies f_r between 401 MHz and 201 MHz that we used as carrier frequencies. For each inductors, the top gate voltage V_{tg} was swept and both the DC conductivity and the reflective RF signal were measured as shown in Fig. 3. We noticed that for $f_c \gg 326$ MHz and despite having a clear DC signal, no reflective signal was observed. This is a consequence of the too high value of the parasitic capacitance and consequently a gate impedance much lower than the matching circuit impedance. However, an rf response is clearly observed for frequencies lower than 306 MHz. One can find out that the impedance of the parasitic capacitance decreases as the probing frequency increases allowing determining an upper bound for the usable probing frequency in our rf setup. We should underline that all measurements have been performed under relatively good matching conditions with the depth of resonant dip exceeding 7 dB, which indicates that the impedance matching mostly affects the measurement sensitivity and not the ability to perform reflectivity measurements itself.

Despite the parasitic capacitance in device 2 being reduced compared with even larger devices ($C_p \approx 0.6$ pF for a device with a top gate of $4 \times 10^2 \mu\text{m}^2$), it still remains an issue for measurements requiring a high sensitivity. To mitigate this, we used the smallest gate area device (device 1) for which $C_p \sim 0.26$ pF for the remaining experiments. We first check the ability to independently adjust the f_r and the sensibility of the reflectometry circuit by mapping out the variation of the reflection coefficient S_{11} in terms of V_t and V_m over the range 0 to 10 V. As expected the resonance amplitude, and so the quality factor Q of the matching circuit, changes with V_m without significantly affecting the resonant frequency value f_r ³². We then selected a reduced range of varactor voltages and optimised the S_{11} parameter to obtain best matching condition among our measurements (see S2). We observe two set of possible voltage values (V_t, V_m) for which the ΔS_{11} value is maximum (Fig. 4(a)). Despite V_t being able to improve the matching, it mostly controls f_r due to its proximity to the circuit. On the contrary, C_m is located upfront of the matching input point, making it more suitable and more efficient for matching purposes. Best matching is obtained for $V_m = 1.5$ V, $V_t = 5$ V, corresponding to $C_t = 6$ pF and $C_m = 5.5$ pF and giving a reflective signal depth of 63 dB. With the view of increasing the measurement sensitivity, namely the quality factor, a higher value for the inductor would be needed but this would ultimately

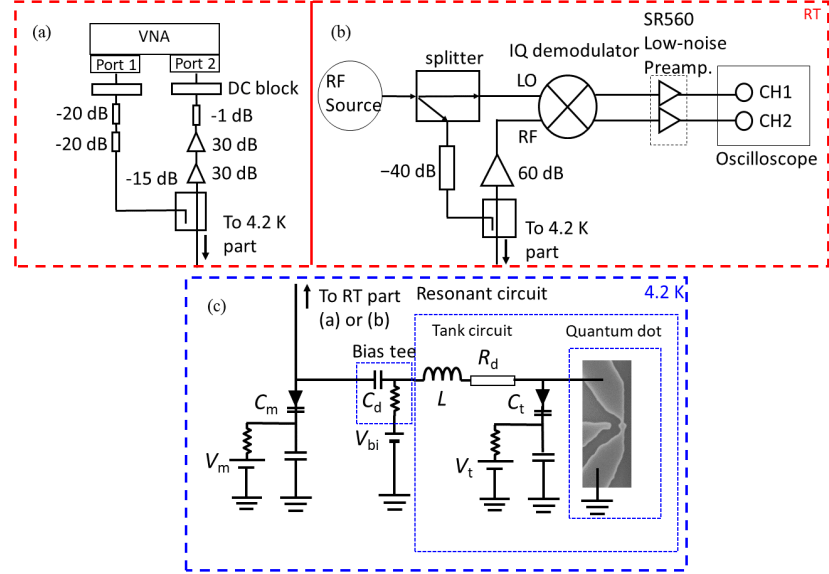


FIG. 2. Measurement setup. (a) Room temperature part of the circuit used for the resonant frequency f_r dependence measurement. The rf signal at 0 dBm is first attenuated before entering a directional coupler and being sent to the quantum dot via the resonant circuit at low temperature. The reflected signal is then amplified at high gain before being measured at the port 2 of the vector network analyzer (VNA). (b) Room temperature part of the circuit used to readout the charge state. Here, the signal from the rf source is split between the incident signal sent directly to the device at low temperature and the demodulator for the measurement of the in-phase (I) and quadrature (Q) components of the reflected signal. (c) The resonant circuit with an inductor of 277 nH together with the two varactors C_m and C_t . R_d represents the losses in the measurement system including the dielectric losses in the device, the printed circuit board (PCB), and in tuning the varactors.

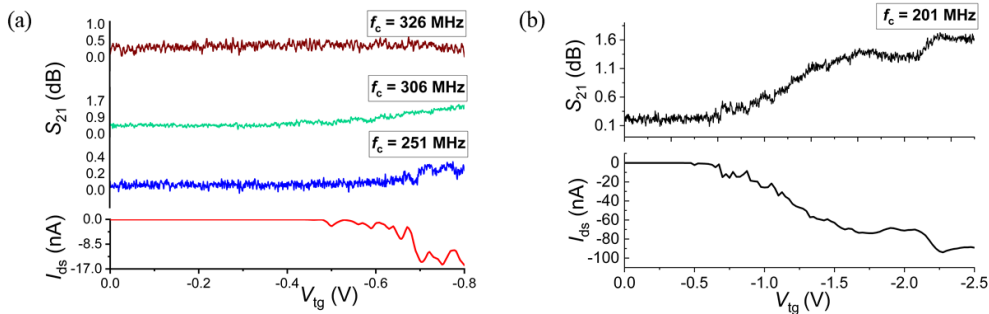


FIG. 3. The rf response of various resonant frequencies. (a) Reflectivity response S_{21} together with the corresponding DC current as a function of the top gate voltage V_{tg} at 4.2 K. (b) Comparison of the rf and DC responses in the accumulation, depletion and inversion regions.

reduce the bandwidth and introduce unintentionally inductor self-resonances around the carrier frequency.

In order to correlate the depth of the impedance matching to the SNR, we set $V_t = 5$ V and adjusted the value of the top gate to the maximum of the transconductance, i.e. -1.85 V (Fig. 4(b)). We then applied a small ac-signal of amplitude 10 mV rms and frequency 3 kHz on the top gate and observed the amplitude modulation (AM) spectrum of the quantum

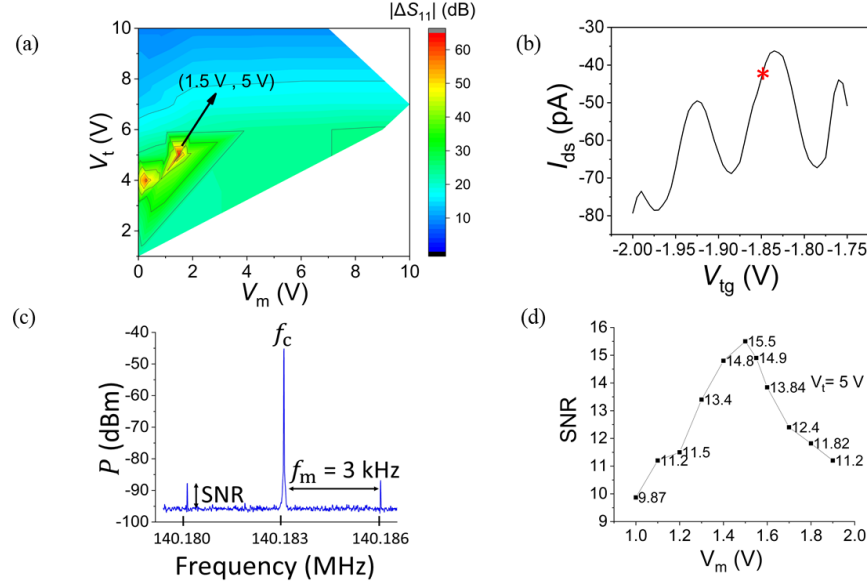


FIG. 4. (a) Variation of the reflection's magnitude as a function of varactor voltages V_m vs V_t . Best matching point is obtained for $V_m = 1.5 \text{ V}$ ($\sim 5.5 \text{ pF}$) and $V_t = 5 \text{ V}$ ($\sim 6 \text{ pF}$) giving a maximum reflective depth of 63 dB for ΔS_{11} (b) Gate oscillations for device 1 as a function of top gate voltage at 4.2 K with $V_t = 5 \text{ V}$ and $V_m = 1 \text{ V}$. The operating point was set to the maximum transconductance ($V_{tg} = -1.85 \text{ V}$) for the SNR measurements in order to achieve the maximum sensitivity. (c) Modulation spectrum showing the 3 kHz sidebands due to the modulating signal (f_m) of amplitude 10 mV rms applied to the top gate. (d) Variation of the SNR with V_m at $V_t = 5 \text{ V}$ showing a maximum value at $V_m = 1.5 \text{ V}$.

dot prior demodulation. The visibility of the sidebands at $f_c \pm 3 \text{ kHz}$ allows determining the SNR value (Fig. 4(c)). By setting $V_t = 5 \text{ V}$ and adjusting the value of the top gate to the maximum of the transconductance, i.e. -1.85 V (Fig. 4(b)), we were able to obtain the variation of the measurement sensitivity as a function of V_m while keeping the resonant frequency unaffected. As observed previously, the maximum SNR is obtained at $V_m = 1.5 \text{ V}$ implying the best matching condition (Fig. 4(d)). We perform rf measurement for three different matching conditions to see the progress in the sensitivity. In the first matching condition, Coulomb diamonds are not seen (Fig. 5(a)). In the second matching condition, Coulomb diamonds can barely be seen (Fig. 5(b)). In the last matching condition, which is the best condition, the diamonds are seen clearly (Fig. 5(c)). These results confirm the increase in SNR as the matching conditions become better.

As a conclusion, we have determined an upper bound for usable frequency in our rf reflectometry setup above which the gate impedance becomes sufficiently small and the rf leakage to the ground gets dominant. By tuning the frequency into the appropriate range and by using two GaAs-based varactors to alleviate the stray capacitance, tune the resonant frequency and improve the matching condition of the circuit, we were able to perform an rf readout of physically defined p-channel silicon quantum dots. Under best matching condition and optimum SNR, we successfully observed Coulomb diamonds at 4.2 K. This study underlines the necessity of carefully designing the device structure in order to achieve high measurement sensitivity and increase the operability of the rf reflectometry. The

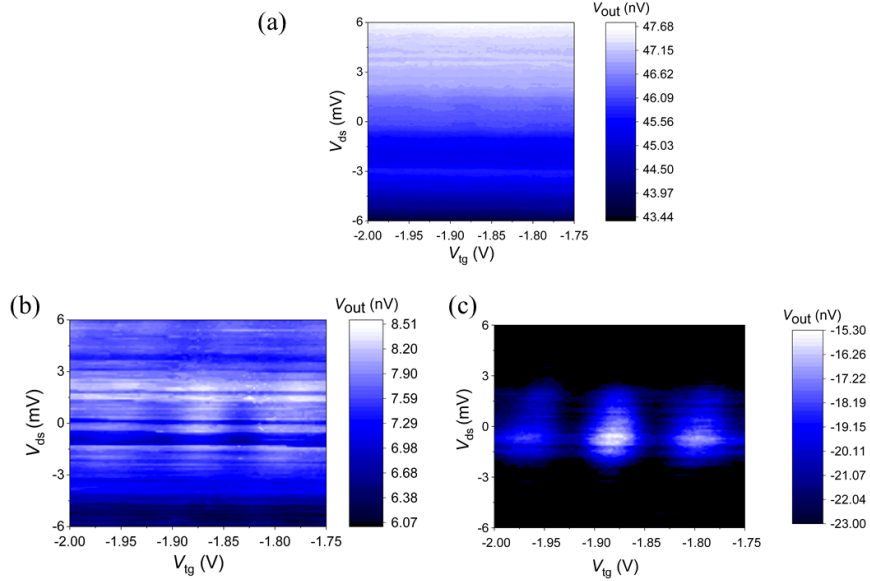


FIG. 5. Charge stability diagram of device 1 obtained by rf reflectometry for three different impedance matching conditions. (a) Both varactors are turned off, (b) Impedance matching is away from best matching ($V_m = 1.1$ V, $V_t = 5$ V), (c) Best matching condition ($V_m = 1.5$ V, $V_t = 5$ V)

addition of the two varactors in the circuit allows the necessary tuning flexibility which will be required in a multi-qubit platform, where frequency multiplexing is expected to be used for both addressing and readout and crosstalks unavoidable. The demonstration of optimised circuitry at 4.2 K is promising for future high temperature operation of quantum bits.

ACKNOWLEDGMENTS

S. B. would like to thank M. F. Gonzalez-Zalba, J. Yoneda, and H. Takahashi for helpful discussion. S. B. also thanks the Hitachi Cambridge Laboratory for the hospitality. This work was partly supported by JST CREST (JPMJ CR1675), JSPS KAKENHI (Grant Numbers JP18K18996 and JP20H00237), MEXT Quantum Leap Flagship Program (Q-LEAP) Grant Number JPMXS0118069228, JST Moonshot R-D Grant Number JPMJMS2065 as well as MEXT Project for Developing Innovation Systems.

- ¹M. Veldhorst, J. C. C. Hwang, C. H. Yang, A. W. Leenstra, B. de Ronde, J. P. Dehollain, J. T. Muhonen, F. E. Hudson, K. M. Itoh, A. Morello, and A. S. Dzurak, *Nature Nanotechnology* **9**, 981 (2014).
- ²N. W. Hendrickx, D. P. Franke, A. Sammak, G. Scappucci, and M. Veldhorst, *Nature* **577**, 487 (2020).
- ³V. S. Pribiag, S. Nadj-Perge, S. M. Frolov, J. W. G. van den Berg, I. van Weperen, S. R. Plissard, E. P. A. M. Bakkers, and L. P. Kouwenhoven, *Nature Nanotechnology* **8**, 170 (2013).
- ⁴B. Voisin, R. Maurand, S. Barraud, M. Vinet, X. Jehl, M. Sanquer, J. Renard, and S. De Franceschi, *Nano letters* **16**, 88 (2016).
- ⁵R. Li, F. E. Hudson, A. S. Dzurak, and A. R. Hamilton, *Nano letters* **15**, 7314 (2015).
- ⁶R. Maurand, X. Jehl, D. Kotekar-Patil, A. Corra, H. Bohuslavskyi, R. Laviéville, L. Hutin, S. Barraud, M. Vinet, M. Sanquer, *et al.*, *Nature communications* **7**, 1 (2016).
- ⁷P. Szumniak, S. Bednarek, B. Partoens, and F. M. Peeters, *Phys. Rev. Lett.* **109**, 107201 (2012).
- ⁸N. M. Zimmerman, W. H. Huber, A. Fujiwara, and Y. Takahashi, *Applied Physics Letters* **79**, 3188 (2001).
- ⁹M. Veldhorst, H. Eenink, C. Yang, and A. S. Dzurak, *Nature communications* **8**, 1 (2017).
- ¹⁰L. Vandersypen, H. Bluhm, J. Clarke, A. Dzurak, R. Ishihara, A. Morello, D. Reilly, L. Schreiber, and M. Veldhorst, *npj Quantum Information* **3**, 1 (2017).
- ¹¹M. Gonzalez-Zalba, S. de Franceschi, E. Charbon, T. Meunier, M. Vinet, and A. Dzurak, arXiv preprint arXiv:2011.11753 (2020).

¹²In the first case, traditional transimpedance amplifiers are structurally limited to bandwidths of a few kilohertz due to a large input resistance and capacitance³⁸. Also one has to manage the intrinsic trade-off between output gain and bandwidth, with III-V amplifiers giving the highest speed while silicon based amplifiers generally providing a better gain. For the second case, the restriction lies in the length of cable that, all quality considered, has a capacitance in excess of 70 pF/m³⁹. Finally, device geometry and structure play a significant part in the reduction in bandwidth. For example, tunnel barrier-based sensors require resistances of a few h/e² for the observation of high quality Coulomb blockade oscillations that are used for monitoring of the charge state or for spin-to-charge conversion⁴⁰.

¹³R. J. Schoelkopf, P. Wahlgren, A. A. Kozhevnikov, P. Delsing, and D. E. Prober, *Science* **280**, 1238 (1998).

¹⁴H. Qin and D. A. Williams, *Applied physics letters* **88**, 203506 (2006).

¹⁵M. Cassidy, A. Dzurak, R. Clark, K. Petersson, I. Farrer, D. Ritchie, and C. Smith, *Applied Physics Letters* **91**, 222104 (2007).

¹⁶D. Reilly, C. Marcus, M. Hanson, and A. Gossard, *Applied Physics Letters* **91**, 162101 (2007).

¹⁷A. Noiri, K. Takeda, J. Yoneda, T. Nakajima, T. Kodera, and S. Tarucha, *Nano Letters* **20**, 947 (2020).

¹⁸J. Colless, A. Mahoney, J. Hornibrook, A. Doherty, H. Lu, A. Gossard, and D. Reilly, *Physical review letters* **110**, 046805 (2013).

¹⁹K. Petersson, C. Smith, D. Anderson, P. Atkinson, G. Jones, and D. Ritchie, *Nano letters* **10**, 2789 (2010).

²⁰A. Crippa, R. Ezzouch, A. Aprá, A. Amisse, R. Laviéville, L. Hutin, B. Bertrand, M. Vinet, M. Urdampilleta, T. Meunier, *et al.*, *Nature communications* **10**, 1 (2019).

²¹M. Schroer, M. Jung, K. Petersson, and J. R. Petta, *Physical review letters* **109**, 166804 (2012).

²²M. Urdampilleta, A. Chatterjee, C. C. Lo, T. Kobayashi, J. Mansir, S. Barraud, A. C. Betz, S. Rogge, M. F. Gonzalez-Zalba, and J. J. Morton, *Physical Review X* **5**, 031024 (2015).

²³M. Gonzalez-Zalba, S. Barraud, A. Ferguson, and A. Betz, *Nature communications* **6**, 1 (2015).

²⁴I. Ahmed, J. A. Haigh, S. Schaal, S. Barraud, Y. Zhu, C. M. Lee, M. Amado, J. W. A. Robinson, A. Rossi, J. J. L. Morton, and M. F. Gonzalez-Zalba, *Phys. Rev. Applied* **10**, 014018 (2018).

²⁵S. Schaal, I. Ahmed, J. Haigh, L. Hutin, B. Bertrand, S. Barraud, M. Vinet, C.-M. Lee, N. Stelmashenko, J. Robinson, *et al.*, *Physical Review Letters* **124**, 067701 (2020).

²⁶In double gate stack devices, the top gate is generally large as it is used to create the inversion layer at the Si-SiO₂ interface and provide conduction to the device whereas the underlying set of gates only aim at creating tunnel barriers and adjusting the tunneling rates.

²⁷T. Nakagawa, T. Sekigawa, T. Tsutsumi, E. Suzuki, and H. Koike, in *2003 Nanotechnology Conference and Trade Show-Nanotech 2003* (2003) pp. 330–333.

²⁸E. J. Connors, J. Nelson, and J. M. Nichol, *Physical Review Applied* **13**, 024019 (2020).

²⁹Y.-Y. Liu, S. Philips, L. Orona, N. Samkharadze, T. McJunkin, E. MacQuarrie, M. Eriksson, L. Vandersypen, and A. Yacoby, *arXiv preprint arXiv:2012.14560* (2020).

³⁰S. Bugu, S. Nishiyama, K. Kato, Y. Liu, T. Mori, and T. Kodera, *Japanese Journal of Applied Physics* **60**, SBB107 (2021).

³¹D. J. Ibberson, T. Lundberg, J. A. Haigh, L. Hutin, B. Bertrand, S. Barraud, C.-M. Lee, N. A. Stelmashenko, J. W. A. Robinson, M. Vinet, M. F. Gonzalez-Zalba, and L. A. Ibberson, *arXiv preprint arXiv:2004.00334* (2020).

³²N. Ares, F. Schupp, A. Mavalankar, G. Rogers, J. Griffiths, G. Jones, I. Farrer, D. Ritchie, C. Smith, A. Cottet, *et al.*, *Physical Review Applied* **5**, 034011 (2016).

³³D. J. Ibberson, L. A. Ibberson, G. Smithson, J. A. Haigh, S. Barraud, and M. F. Gonzalez-Zalba, *Applied Physics Letters* **114**, 123501 (2019).

³⁴T. Müller, B. Küng, S. Hellmüller, P. Studerus, K. Ensslin, T. Ihn, M. Reinwald, and W. Wegscheider, *Applied Physics Letters* **97**, 202104 (2010).

³⁵T. Kambara, T. Kodera, Y. Arakawa, and S. Oda, *Japanese Journal of Applied Physics* **52**, 04CJ01 (2013).

³⁶K. Horibe, T. Kodera, and S. Oda, *Applied Physics Letters* **106**, 053119 (2015).

³⁷Y. Yamaoka, K. Iwasaki, S. Oda, and T. Kodera, *Japanese Journal of Applied Physics* **56**, 04CK07 (2017).

³⁸M. Manoharan, Y. Tsuchiya, S. Oda, and H. Mizuta, *Nano letters* **8**, 4648 (2008).

³⁹G. Gautschi, *Piezoelectric Sensorics: Force Strain Pressure Acceleration and Acoustic Emission Sensors Materials and Amplifiers. 2013* (Springer Berlin Heidelberg) p. 236.

⁴⁰J. J. M. Elzerman, R. Hanson, J. S. Greidanus, L. H. W. van Beveren, S. D. Franceschi, L. M. K. Vandersypen, S. Tarucha, and L. P. Kouwenhoven, *Phys. Rev. B* **67**, 161308(R) (2003).